ORIGINAL ARTICLE

Characterization of Passive Films Formed on As-received and Sensitized AISI 304 Stainless Steel

Yubo Zhang[1,2,3,4] , Hongyun Luo[1,2,3*], Qunpeng Zhong[1,2,3], Honghui Yu[1,2,3] and Jinlong Lv[4,5]

Abstract

The current research of corrosion resistance of stainless steels mainly focuses on characterization of the passive films by point defect mode and mixed-conduction model. The corrosion resistance of the passive films formed on as-received and sensitized AISI304 stainless steel in borate buffer solution were evaluated in this paper. The degree of sensitization and corrosion resistance of AISI304 stainless steels was evaluated by double loop electrochemical potentiodynamic reactivation and electrochemical impedance spectroscopy. The passive films formed on the stainless steels were studied by XPS technique. It was found that as-received specimen had higher pitting corrosion potential and corrosion resistance than sensitized one. The Mott-Schottky results showed that sensitized stainless steel had more defects in the passive film than as-received one. The compositions of the passive films were mainly Cr and Fe oxides according to XPS results.

Keywords: 304 stainless steel, Sensitization, Passive films, XPS, Impedance

1 Introduction

Austenitic stainless steels are widely used in components designed for high temperature applications like nuclear power stations, superheaters, and thermal power plant [1]. However, some localized corrosion such as pitting corrosion [2, 3], intergranular corrosion [4], stress corrosion crack (SCC) [5, 6] were often observed especially in the temperature range of 450–900 °C. The chromium carbides ($Cr_{23}C_6$) are is easily precipitated and resulted into sensitization in the grain boundaries. The depletion zone in which chromium concentration is less than 12 wt.% making the material vulnerable to corrosion [7]. The corrosion resistance of stainless steels is basically controlled by the protection of the surface oxide layer. The destruction of the passive films on stainless steels will induce SCC [8–10]. Therefore, further understanding the compositions and physical characteristics of the passive films formed on the stainless steels could probably help us to clarify corrosion mechanism.

The integrity of the passive film on stainless steel changes with its environment. Many factors may affect the properties of the passive film, such as temperature [11, 12], applied potential [13], solution pH [14], time [14], ion concentration of the electrolyte [15], the composition [16] and heat treatment conditions of the materials [17]. The sensitized 316 stainless steel showed a wide range of potential for cracking and a transition from transgranular to intergranular cracking with the increasing of applied potential [18]. At a lower potential below the Flade potential, oxides of Fe^{2+} were formed in the passive region for Fe-Cr alloys. Fe^{2+} was oxidized to Fe^{3+} with increasing of the potential above the Flade potential. Moreover, the oxides of Cr^{3+} were changed into hexavalent chromium with a further increase in the potential [19, 20]. Kocijan et al. [21] found that the presence of molybdenum enhanced the corrosion resistance of 316L stainless steel due to the formation of Cr_2O_3 and CrO_3 in the passive film. However, high chromium and molybdenum content induced also secondary phases and reduced the pitting potential

*Correspondence: luo7128@163.com
[1] Key Laboratory of Aerospace Materials and Performance (Ministry of Education), School of Materials Science and Engineering, Beijing University of Aeronautics and Astronautics, Beijing 100191, China
Full list of author information is available at the end of the article

Zhang *et al. Chin. J. Mech. Eng.*   (2019) 32:27

Page 2 of 12

value of Alloy 900. The main components in the passive film were chromium and iron oxides based on some test methods, such as XPS, non-destructive hard X-ray photoelectron spectroscopy (HAXPES) and angular resolved X-ray photoelectron spectroscopy (ARXPS) [11, 22]. The thickness of the passive film can also be determined by XPS and Auger electron spectroscopy (AES) [23].

The heat treatment of components for stress relief could result in a sensitization. The intergranular corrosion is easy to occur in sensitized sample. Therefore, it is important to study the effect of sensitization on the stability of the passive films. The degree of sensitization (DOS) increases with the duration for 304H stainless steel in the range 550 °C to 750 °C. DOS increased and decreased thereafter for 304H stainless steel at 800 °C due to self healing [24]. Secondary phase presence induced by sensitization reduces the pitting potential value of Alloy 900. And the corrosion potential and open circuit potential increased due to higher temperature and sensitization [7]. DOS of the austenitic stainless steel can be distinguished clearly from the AC impedance response of the specimens when they are polarized in the middle of transpassive potential region [25]. Besides, the electrochemical impedance spectroscopy (EIS) method is widely used to characterize the oxide films formed on metals and alloys. It is also possible to obtain the information on the mechanism and the film growth model based on EIS analysis. Hamadou et al. [26] investigated thermally formed oxide films on AISI 304L stainless steel by impedance.

Therefore, the AISI 304 austenitic stainless steel is studied in borate buffer solution at pH 9.2. The effects of applied potential and sensitization on the protection of passive films on the specimens were studied by electrochemical techniques of potentiodynamic polarization, cyclic voltammetry and electrochemical impedance spectroscopy (EIS). The difference of semiconducting properties between as-received and sensitized specimens also was evaluated by Mott–Schottky measurement. In addition, the compositions of the passive films formed on the steels at special potentials were studied by XPS technique. Finally, the oxygen vacancy diffusivity was calculated using the point defect model (PDM), and then the impedance response was certificated according to PDM.

2 Materials and Experimental

2.1 Specimen Preparation

The chemical compositions of initial AISI 304 austenitic stainless steel plate with the 2 mm thickness is are shown in Table 1. Some of the samples were heated for 5 h at 675 °C followed with water quenched. The samples were cut to cuboid with a dimension of 10 mm × 10 mm × 2 mm for test. Prior to the electrochemical studies the electrode surface was polished with 3000 SiC sandpaper, cleaned with distilled water and acetone, and then dried in air.

2.2 Electrochemical Procedure

A conventional three-electrode electrochemical cell and CHI 660B electrochemical station (Chenhua Instrument Co. Shanghai, China) were used. Two graphite counter electrode and a saturated calomel reference electrode (SCE) were used. The experiment was carried out in 0.05 M H_3BO_3 + 0.075 M $Na_2B_4O_7 \cdot 10H_2O$ (pH ≈ 9.2) borate buffer solution at ambient temperature. The degree of sensitization (DOS) values of both specimens was measured by double loop electrochemical potentiodynamic reactivation (DL-EPR) technique in 0.5 M H_2SO_4 + 0.01 M KSCN solution, and then microstructure was observed by Scanning Electron Microscope (SEM).

Before each measurement the electrode was polarized cathodically at −1.0 V_{SCE} for 5 min to remove the natural passive films on the surface [27]. The potentiodynamic polarization tests were carried out at 1.67 mV/s and the potential range from −1.2 V_{SCE} to 1.0 V_{SCE}. The cyclic voltammetry were recorded, starting at −1.0 V_{SCE}, using different scan rate, until the transpassive region was reached. Before the EIS measurements, the specimens firstly were polarized at −0.2 V_{SCE}, 0 V_{SCE}, 0.2 V_{SCE}, 0.4 V_{SCE}, 0.6 V_{SCE} and 0.8 V_{SCE}, respectively, for 1 h to ensure the formation of stable enough films. These potentials were chosen with reference to the characteristic features of the polarization curve. The EIS was measured in the frequency range from 100 kHz to 10 mHz with AC amplitude of 10 mV (rms). Zsimpwin software was used to fit the EIS experiment data. Capacitance values were calculated from the imaginary part of impedance. The Mott–Schottky plots were obtained by sweeping in negative direction at constant frequency of 1000 Hz, with an amplitude signal of 5 mV. The potential range from 1.0 V_{SCE} to −1.2 V_{SCE} with 20 mV potential step.

Table 1 Chemical compositions (wt.%) of AISI 304 stainless steel

C	Si	Mn	P	S	Cr	Ni	Fe
0.05	0.84	1.80	0.024	0.024	17.35	9.12	Balance

Zhang *et al. Chin. J. Mech. Eng.*   (2019) 32:27

Page 3 of 12

2.3 Complementary Characterizations

The morphologies and stainless steel were characterized by a field emission scanning electron microscopy (FE-SEM) of LEO-1530). The compositions of passive films formed on stainless steel were measured by XPS. The XPS experiments were carried out using PHI Quantera SXM (ULVAC-PHI, INC). Photoelectron emission was excited by monochromatic Al $K\alpha$ radiation. XPSPeak4.1 software was used to fit the XPS experiment data.

3 Results and Discussion

3.1 Microstructural Analysis

DOS value of sensitized specimen is 0.3499 while the as-received specimen is 0. The microstructures after the measurements of DOS are shown in Figure 1. It can be seen that as-received specimen shows almost no ditches in grain boundaries, whereas a considerable number of ditches occur on sensitized specimens. Certain precipitates, which were mainly $Cr_{23}C_6$, were formed along grain boundaries, displaying a lower chromium value than the value inside the grain. Therefore, chromium depleted region deteriorates the corrosion resistance of the passive films.

3.2 Polarization Measurements

Figure 2 shows the potentiodynamic plots of AISI 304 stainless steel in borate buffer solution. Both of them display anodic polarization characteristic. The corrosion potential was -0.468 V_{SCE} for as-received specimen and -0.42 V_{SCE} for sensitized specimen, a little positive than as-received specimen. Besides, sensitized specimen has a little lower pitting corrosion potential than the as-received one. The passive range for both specimens were almost the same, from -0.38 $V_{SCE} \sim 0.92$ V_{SCE}. This implies that precipitated $Cr_{23}C_6$ along grain boundaries did affect the passivation behavior of the Cr depletion zone, which will be demonstrated by EIS and Mott-Schotty results, whereas the shape of the polarization curves did not change significantly. It is apparent
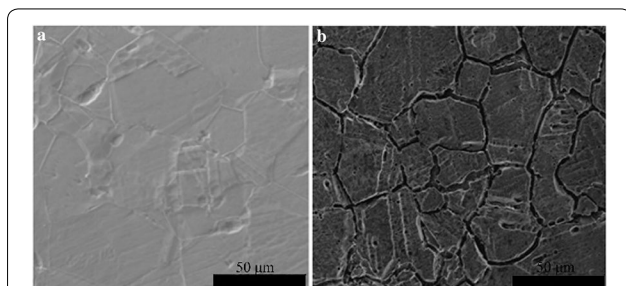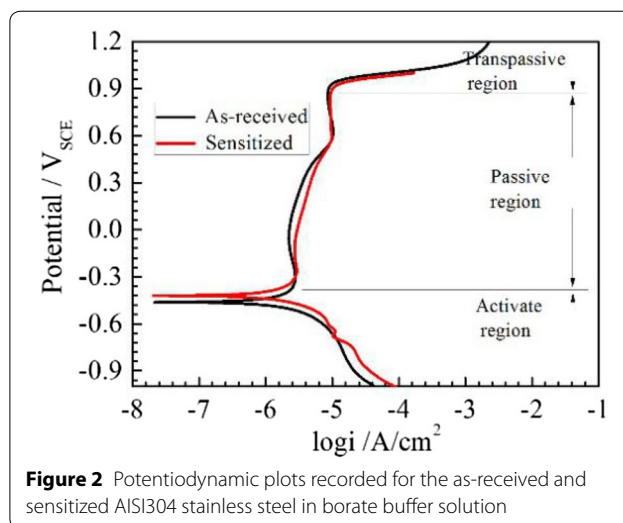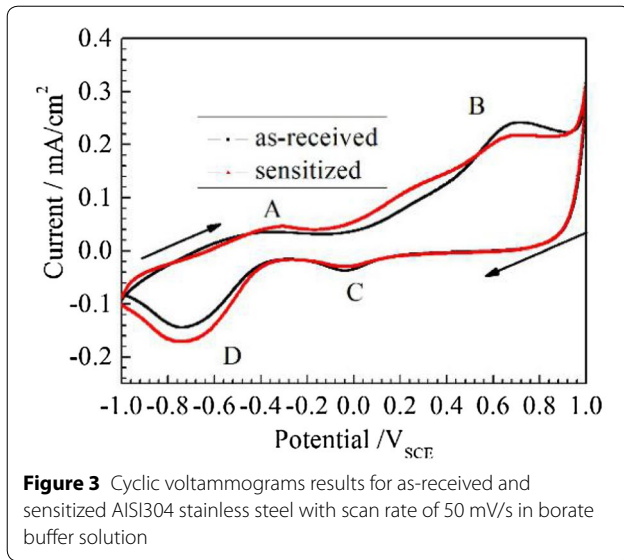

Figure 2 Potentiodynamic plots recorded for the as-received and sensitized AISI304 stainless steel in borate buffer solution

that the curves include evident three regions. The metal starts to oxidize due to increased potential in active region. The oxidation is induced by the increasing of the current density. The metal surface is covered with a passive films which is a barrier layer between the metal and the corrosive environments in passive potential region. Higher passivated potential promotes to form stable passive film with higher oxidation valence. However, oxidation of metal cations also could result in a breakdown of the passive film and initiating unstable pits. Therefore, the passive film comes into the transpassive region and the stable pits appear with the increasing of the current density.

The cyclic voltammetry is utilized for further study. The cyclic potentiodynamic curves of two stainless steel specimens are shown in Figure 3. The anodic and cathodic peaks of the current density appear almost at the same potentials for both specimens. Prior the first anodic peak at -0.4 V_{SCE} (point A), the current density increases with the increasing of the potential due to the formation of Cr^{3+} and Fe^{3+} ions according to Aleksandra Kocijan [21]. Another anodic peak (point B) is observed at 0.67 V_{SCE}. This is probably the oxidation of Cr atoms into Cr^{6+} [21, 28, 29]. First peak in the cathodic cycle (point C) may be the reduction of Cr^{6+}. While the peak at $-0.6 \sim -0.7$ V_{SCE} (point D) could be ascribed to the reduction of Fe^{3+} [21, 29]. In contrast, a slight difference in the values of the current density existed especially at 0.6 and -0.7 V_{SCE}. The reason might be the situation that chromium carbides precipitated in grain boundaries for sensitized specimen and formed chromium-deplete zone, leading to the decrease of oxidation rate of Cr as result of the decrease of current density at 0.6 V_{SCE}. Furthermore, at approximately -0.7 V_{SCE}, the weak zones

Figure 1 SEM microstructures of (**a**) as-received and (**b**) sensitized stainless steels after the measurements of DOS

Zhang *et al. Chin. J. Mech. Eng.* (2019) 32:27

Page 4 of 12

Figure 3 Cyclic voltammograms results for as-received and sensitized AISI304 stainless steel with scan rate of 50 mV/s in borate buffer solution
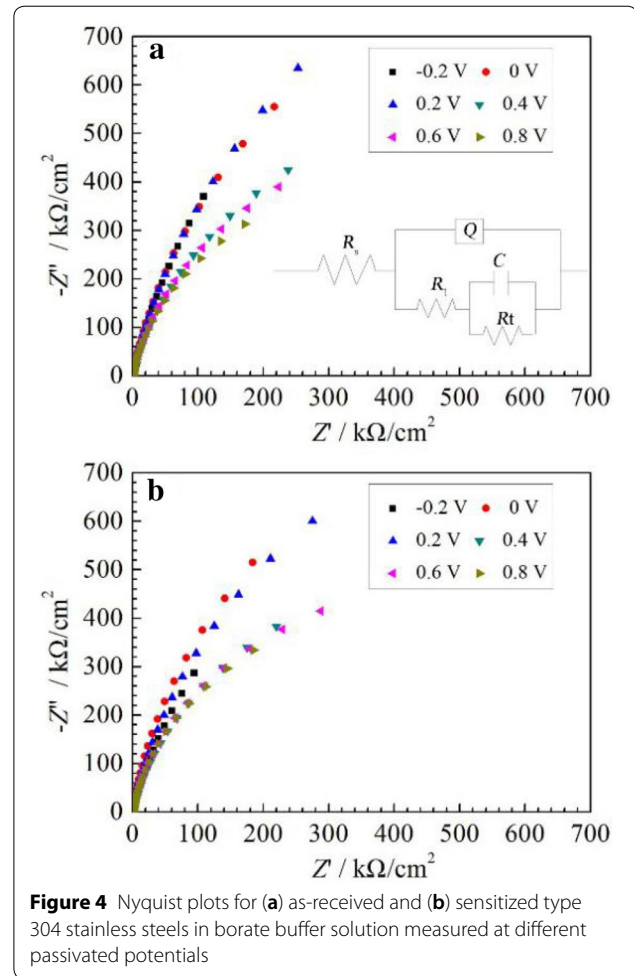
of grain boundaries for sensitized specimen accelerated the reduction of Fe^{3+}, resulting in the increase of current density.

3.3 EIS Measurements

The electrochemical impedance spectroscopy (EIS) is utilized to characterize the electronic properties of passive films on metals and alloys for obtaining information on the electronic structure, mechanism and the passive film growth model. This technique has been used either to propose an equivalent circuit for an electrochemical system.

In order to investigate relative stability of the passive films formed on the steels, EIS measurements are carried out. According to the polarization curves, six potentials in the passive region are chosen for electrochemical impedance analysis. Figure 4 shows the Nyquist plots of both specimens at different applied potentials in borate buffer solution. The impedance is applied potential dependence. However, it is not proportional to the potential, which is different from the regularity of 316L stainless steel in 0.2 M borate buffer solution [17]. The resistances for higher potentials decrease a lot, compared with lower potentials for both as-received and sensitized specimens. The equivalent circuits of Nyquist plots are also presented in Figure 4. In the circuit R_s, R_1 represent the resistance of solution and the charge transfer resistance. R_t is the film resistance and C the double layer capacity. Q is the constant phase element (CPE) considering relaxation times due to heterogeneities at the electrode surface [30, 31]. The impedance of CPE is given by

$$Z_{CPE} = \frac{1}{Q}(j\omega)^n. \tag{1}$$

Figure 4 Nyquist plots for (**a**) as-received and (**b**) sensitized type 304 stainless steels in borate buffer solution measured at different passivated potentials

Therefore, the total impedance is

$$Z_{total} = R_{sol} + \left(Q(j\omega)^n + \frac{1 + R_t Cj\omega}{R_1 + R_t + R_1 R_t Cj\omega} \right)^{-1}, \tag{2}$$

where ω is the angular frequency, n is the exponent of the CPE and always lies between 0.5 and 1. The fitting results are shown in Table 2.

As present in Table 2 for as received specimens, the resistance changes at the potential of 0–0.2 V_{SCE} where the current density peak is observed in the cyclic voltammograms. Consequently, a good relationship existed between EIS and cyclic voltammograms. In Figure 5, the resistances of as-received specimens are always higher than sensitized ones at all potentials, which indicates that the corrosion resistance of sensitized specimens decreases due to sensitization. The difference is bigger in lower potentials than in higher potentials. It is probably that the rate of anodic dissolution is slower than the rate of the oxidation of the Fe^{2+} and Cr^{3+}. Besides the resistance of as-received

Table 2 Equivalent circuit for fitting parameters of 304 stainless steel in borate buffer solution

|	Potential E (V)	Resistance of solution R_s (Ω/cm^2)	CPE Q (Ω^{-1}s^n cm^{-2})	Exponent of CPE (n)	Charge transfer resistance R_1 (Ω/cm^2)	Capacity C/F (cm^{-2})	Film resistance R_t (Ω/cm^2)
As-received	-0.2	58.61	2.167×10^{-5}	0.8704	61.07	3.84×10^{-6}	3.607×10^{-6}
	0	51.14	1.248×10^{-5}	0.8768	26.26	4.208×10^{-6}	3.144×10^{-6}
	0.2	50.59	1.057×10^{-5}	0.8615	23.69	3.527×10^{-6}	3.34×10^{-6}
	0.4	49.34	1.289×10^{-5}	0.8422	18.56	5.209×10^{-6}	1.542×10^{-6}
	0.6	53.74	1.786×10^{-5}	0.8872	24.39	5.866×10^{-6}	1.262×10^{-6}
	0.8	49.14	1.835×10^{-5}	0.8739	24.28	8.065×10^{-6}	1.025×10^{-6}
Sensitized	-0.2	54.11	2.779×10^{-5}	0.8645	71.4	3.783×10^{-6}	2.406×10^{-6}
	0	48.7	1.433×10^{-5}	0.9016	30.97	4.939×10^{-6}	2.378×10^{-6}
	0.2	55.37	1.536×10^{-5}	0.9346	9.523	5.536×10^{-6}	2.104×10^{-6}
	0.4	56.83	1.565×10^{-5}	0.8584	19.46	4.397×10^{-6}	1.32×10^{-6}
	0.6	54.54	1.231×10^{-5}	0.8742	22.65	5.223×10^{-6}	1.136×10^{-6}
	0.8	51.13	1.803×10^{-5}	0.8827	31.27	6.83×10^{-6}	1.005×10^{-6}
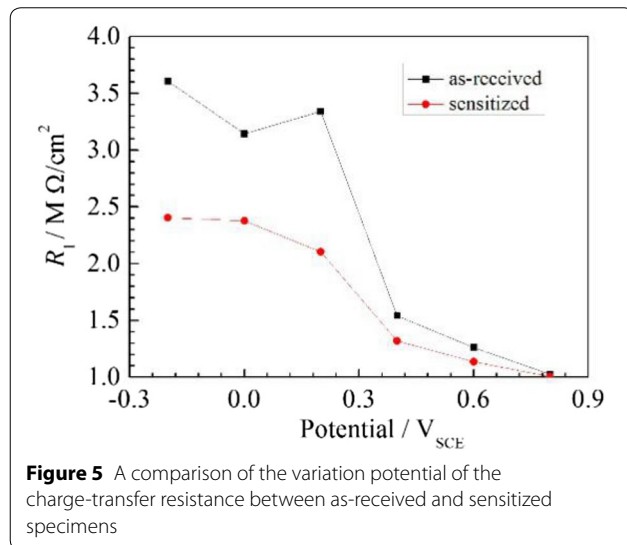
Figure 5 A comparison of the variation potential of the charge-transfer resistance between as-received and sensitized specimens

specimens is not linear relationship with applied potential, which is different to Ref. [32].

3.4 Mott-Schottky Analysis

It is well known that the passive films formed on stainless steels exhibit semiconducting behavior based on the Mott-Schottky analysis [11, 16, 33–36]. Doping density in the passive films can also be calculated by slope of Mott-Schottky results. The capacitance of the passive films can be obtained by Eqs. (3) and (4):
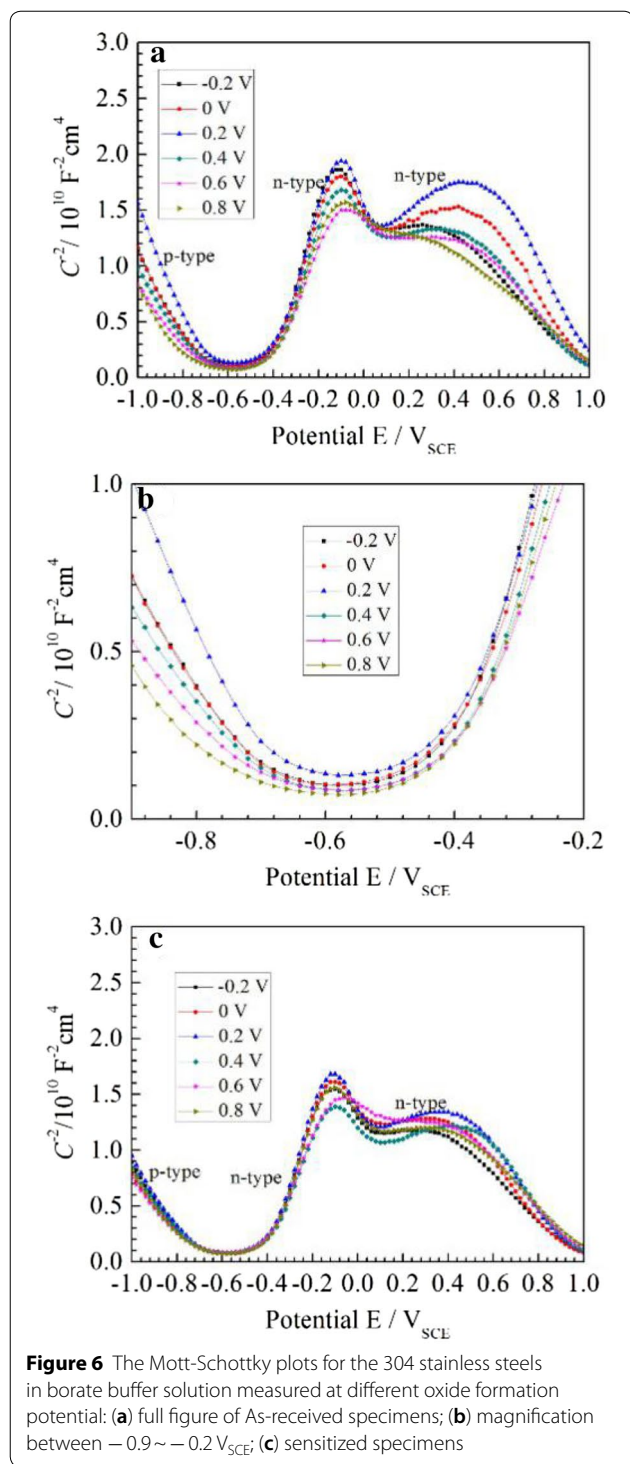
for *n*-type semiconductor

$$\frac{1}{C^2} = \frac{2}{\varepsilon\varepsilon_0 eN_D}\left(E - E_{fb} - \frac{kT}{e}\right), \tag{3}$$

for *p*-type semiconductor

$$\frac{1}{C^2} = -\frac{2}{\varepsilon\varepsilon_0 eN_A}\left(E - E_{fb} - \frac{kT}{e}\right), \tag{4}$$

where E stands for applied potential, ε is the dielectric constant of the passive film ($\varepsilon = 15.6$ [37]), ε_0 is the permittivity of free space (8.854×10^{-14} F/cm), e is the electron charge (1.602×10^{-19} C), N_D and N_A represent the donor and acceptor density and can be determined from the slope of Mott-Schottky plots. E_{fb} is the flat band potential, k is the Boltzmann constant (1.38×10^{-23} J/K), and T is the absolute temperature. The interfacial capacitance C can be obtained by the relation $C = (-2\pi f Z'')^{-1}$ where Z'' is the imaginary part of the impedance and f represents the frequency. The space charge capacitance is very small compared to that of the Helmholtz layer. The capacitance of the space charge region becomes important but is still smaller than that of the Helmholtz layer. Therefore, the capacitance of the double layer can be neglected, and obtained capacitance C is regarded as the space charge capacitance.

As shown in Figure 6(a)–(c), two stainless steel specimens have almost the same flat-band potential of -0.6 V$_{SCE}$. For two specimens the passive film show negative slope at $-1.2 \sim -0.6$ V$_{SCE}$, indicating performs *p*-type semiconductor, while the passive film exhibits positive slope at the potential range of $-0.6 \sim -0.1$ V$_{SCE}$, indicating *n*-type semiconductor property. Variation of *p*-type to *n*-type to *p*-type repeatedly appears at the potentials from -0.1 V$_{SCE}$ to 0.1 V$_{SCE}$, from 0.1 V$_{SCE}$ to 0.4 V$_{SCE}$ and from 0.4 V$_{SCE}$ to 1.0 V$_{SCE}$. The various semiconductor properties may be caused by the compositions of the passive films [36]. The oxygen vacancies and metal interstitials in passive film endow *n*-type characteristic (Fe_2O_3, TiO_2, MoO_3, Fe(OOH), etc.), while cation

Zhang *et al. Chin. J. Mech. Eng.* (2019) 32:27

Page 6 of 12

Figure 6 The Mott-Schottky plots for the 304 stainless steels in borate buffer solution measured at different oxide formation potential: (**a**) full figure of As-received specimens; (**b**) magnification between $-0.9 \sim -0.2\,V_{SCE}$; (**c**) sensitized specimens

vacancies in the passive film endow *p*-type characteristic (Cr_2O_3, MoO_2, $FeCr_2O_4$, NiO, etc). Therefore, *p*-type semiconductor in Figure 6(a)–(c) may come from the Cr oxide and Fe_3O_4 enriched in the inner of the passive film. And the dominant acceptor species are metal vacancies,

V_{Cr}^{3+} [38]. The *n*-type semiconductor is probably due to the formation of Fe_2O_3 and $Fe(OH)_3$ with the dominant donor species of oxygen vacancies. Besides, Fe-Cr spinel may contribute to *n*-type semiconductor [39]. In alkaline solutions oxides of iron are much more stable than oxides of chromium. So oxides of chromium will be preferential to dissolve and the passive films perform *p*-type at potentials higher than $0.5\,V_{SCE}$. The discussion above will be demonstrated by XPS analysis.

The variations of the donor and acceptor densities with potential are shown in Figure 7. It is demonstrated that the slope of Mott-Schotty plots is different from each other at various potentials. The higher in slope indicates lower concentration of defect in the passive film. Corresponding to the impedance spectroscopy, the resistance of the film is larger. As shown in Table 2, the resistance of the passive film decreases from the potential of $0.2\,V_{SCE}$ to $0.6\,V_{SCE}$, at the same time, in Figure 7 N_D increases at the same potential range. The reason is that when the concentration of the defect is lower, space charge layer capacitance is lower and it is difficult for charge to transfer, so the reactions at the interface are unlikely to proceed, which leads to the better corrosion resistance. It is obvious that at specific potential N_A is always higher than N_D. Compared with as-received specimens, the N_D values for sensitized ones are always higher, which means more defects in the film formed on sensitized specimens.
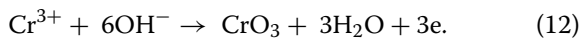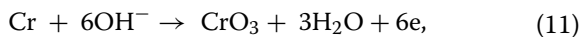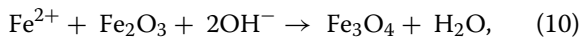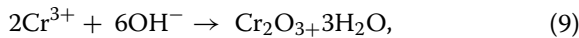
3.5 XPS Analysis

To further demonstrate the results of the cyclic potentiodynamic and Mott-Schotty results, XPS measurements are used to directly characterize the composition of passive film formed on specimens after polarization at two potentials for 1 h. The Cr $2p_{3/2}$, Fe 2p and O1s XPS signals after obtained at $0.2\,V_{SCE}$ and $0.6\,V_{SCE}$ for 1 h are presented in Figure 8a–f. At $0.2\,V_{SCE}$ the main oxides in the passive film are Cr_2O_3, $Cr(OH)_3$, Fe_2O_3 and FeO. This is agreed well with the result of cyclic voltammograms which show higher concentration of Cr^{3+} after the first anodic peak. When the potential increases to $0.6\,V_{SCE}$, CrO_3 appears and results into the second anodic peak. Intensity variation of chromium and iron oxides is different from 316L stainless steel and 304L stainless steel [21, 28]. The fitting parameters for chromium, iron and oxygen were shown in Table 3. The thickness of passive film was estimated to 10 nm, thicker than 316L polarized at $0.6\,V_{SCE}$ in H_2SO_4 [23].

According to the oxides in different potentials, some reactions may be required. Before $0.2\,V_{SCE}$ Fe and Cr dissolve and Fe^{2+} is oxidized to Fe_2O_3, so the passive film performs *n*-type semiconductor property which is agreed with the Mott-Schotty results. The anodic polarization process is as follows:

Zhang *et al. Chin. J. Mech. Eng.* (2019) 32:27

Page 7 of 12

Figure 7 Doping density of the passive film for both specimens between − 0.2 and 0.8 V_{SCE} in borate buffer solution

$$Fe \rightarrow Fe^{2+} + 2e, \tag{5}$$

$$Fe \rightarrow Fe^{3+} + 3e, \tag{6}$$

$$Cr \rightarrow Cr^{3+} + 3e, \tag{7}$$

$$2Fe^{2+} + 6OH^- \rightarrow Fe_2O_3 + 3H_2O + 2e. \tag{8}$$
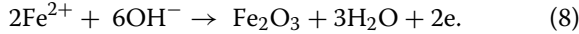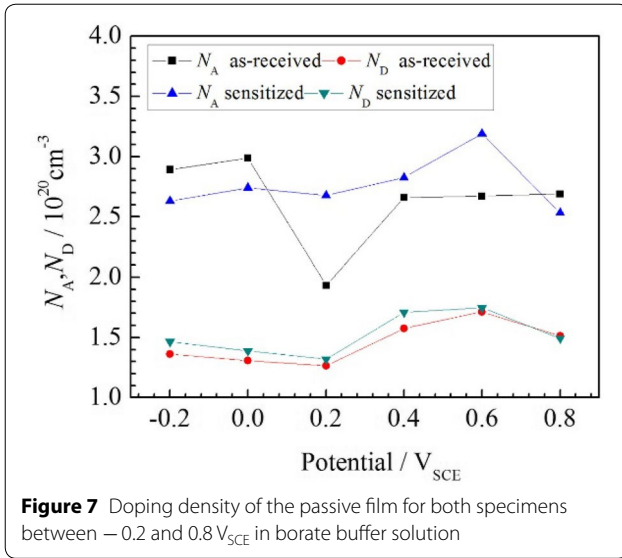
The dissolution of Fe and Cr decreases and the current density increases from 0.2 V_{SCE} to 0.6 V_{SCE}. Therefore, the following reactions may occur:

$$2Cr^{3+} + 6OH^- \rightarrow Cr_2O_3 + 3H_2O, \tag{9}$$

$$Fe^{2+} + Fe_2O_3 + 2OH^- \rightarrow Fe_3O_4 + H_2O, \tag{10}$$

$$Cr + 6OH^- \rightarrow CrO_3 + 3H_2O + 6e, \tag{11}$$

$$Cr^{3+} + 6OH^- \rightarrow CrO_3 + 3H_2O + 3e. \tag{12}$$

Reactions above demonstrate that the passive films are constituted by Cr_2O_3 and Fe_3O_4, which makes the passive film behave *p*-type semiconductor. The conclusion is also precisely consistent with the Mott-Schotty results [40, 41].

3.6 Diffusivity of Defects

The migration of point defects is a key parameter which can be evaluated by the diffusivity of the point defects (D_0) based on the Mott-Schotty results and PDM theory. The dominant donor species in *n*-type semiconductor are oxygen vacancies and metal interstitials. As shown in Figure 8(c) and (d), the intensity of FeO at 0.2 V_{SCE} and 0.6 V_{SCE} are almost the same, so we can assume that the content of metal interstitials remains unchanged at different

potentials and oxygen vacancy is the dominant role during the transport of point defects. Consequently, oxygen vacancy diffusivity can be calculated according to PDM [42].

The relationship between them is as following based on PDM:

$$N_D = \omega_1 \exp(-bV_{ff}) + \omega_2, \tag{13}$$

$$\omega_2 = -\frac{J_0}{2KD_0}, \tag{14}$$

where V_{ff} is the applied potential, ω_1, ω_2 and b is the unknown parameters [43]. The values of the parameters can be calculated by the fitting curve of donor densities of the passive films. The diffusivity can be acquired from Eq. (15):

$$D_0 = -\frac{J_0}{2\omega_2 K}, \quad K = F\varepsilon_L/RT, \tag{15}$$

where ε_L represents the electric field strength, J_0 is the flux of the defect, F is Faraday constant, R is gas constant and T is temperature.

For *n*-type semiconductor, J_0 is determined by the flux of oxygen, so J_0 could be expressed as [43]:

$$J_0 = -\frac{i_{ss}}{2e}, \tag{16}$$

where i_{ss} is the steady-state current density.

According to PDM [42],

$$L_{SS} = \frac{1}{\varepsilon_L}(1 - \alpha)V_{ff} + B, \tag{17}$$

where α is the polarizability of the film/solution interface, assuming $\alpha = 0.5$, B is a constant.

In the high electric field model field strength, ε_{HFM} satisfies the following equation:

$$\frac{1}{\varepsilon_{HFM}} = \frac{1 - \alpha}{\varepsilon_L}. \tag{18}$$

Consequently, substituting Eqs. (15)–(18) into Eq. (14) yields

$$D_0 = \frac{i_{ss}RT}{4\omega_2 eF\varepsilon_L}. \tag{19}$$

Substitution of the values into Eq. (19) yields $D_0 = 5.69 \times 10^{-17}$ cm^2/s. Considering the uncertainty in α and ε_L, the obtained diffusivity of oxygen vacancies in the passive films in the present study is in the range of 10^{-16}–10^{-17} cm^2/s.

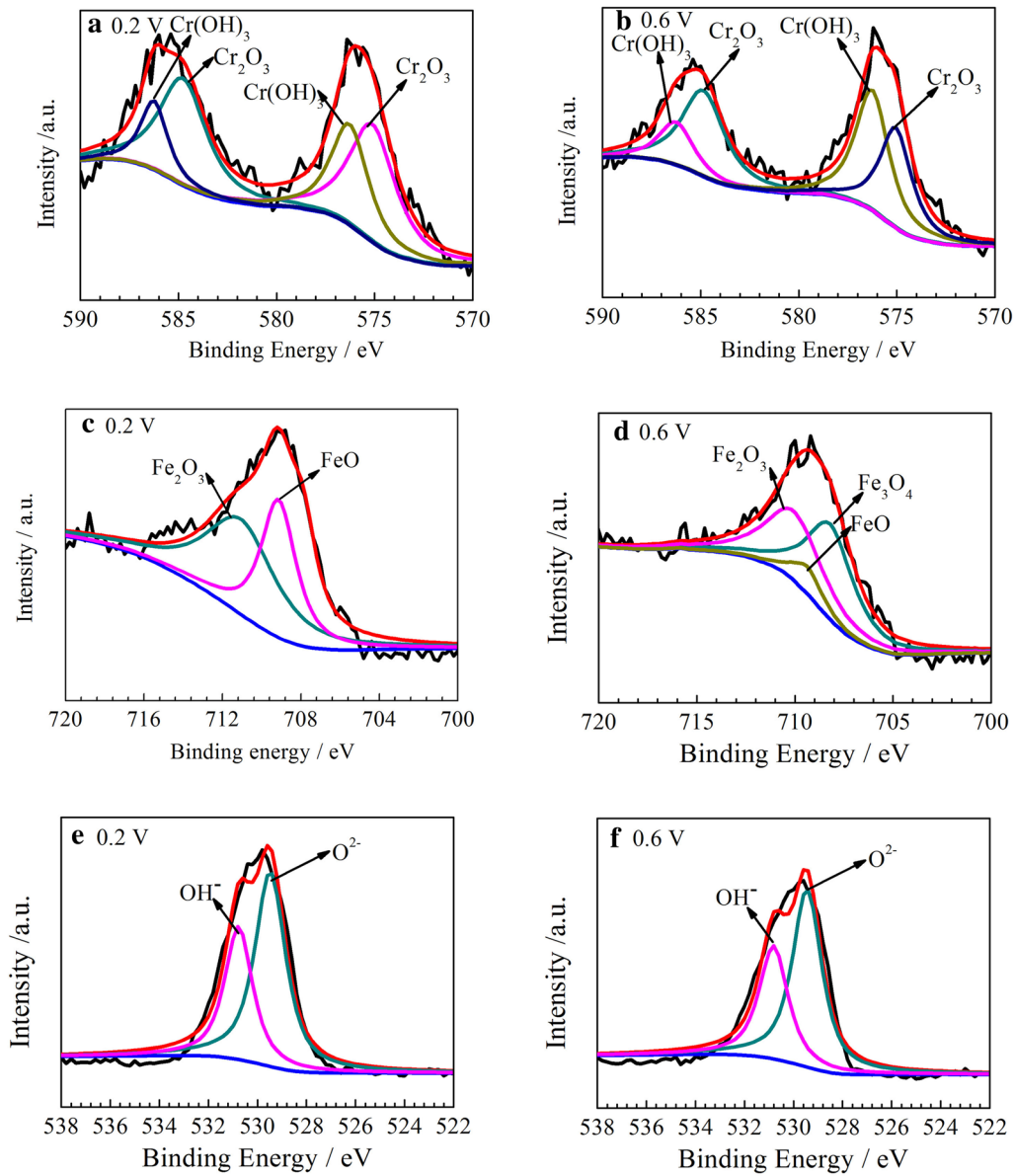Zhang *et al. Chin. J. Mech. Eng.*   (2019) 32:27

Page 8 of 12

Figure 8 The detailed XPS spectra of (**a**, **b**) Cr 2p$_{3/2}$, (**c**, **d**) Fe 2p and (**e**, **f**) O1s of the passive films formed on 304 stainless steels oxidized for 1 h in borate buffer solution

3.7 Impedance Response of Passive films

According to PDM(III) [44, 45] the impedance function in the electrochemical system can be defined as

$$Z = V_{ac}(\omega)/I_{ac}(\omega), \tag{20}$$

where $V_{ac}(\omega)$ and $I_{ac}(\omega)$ are the external AC potential and current, respectively, and ω is the frequency. Equation (20) can also be expressed as

$$Z = \overline{V_{ac}}(t)/\overline{I_{ac}}(t). \tag{21}$$

So the total current of passive film includes electronic current due of electron transport, electronic current of the diffusion of electron holes, ionic current of the transport of oxygen vacancy and ionic current due to the transport of interstitial cation. Thus

$$I_{total} = I_{e'} + I_{h\cdot} + I_{Vo\cdot\cdot} + I_{V_M^{x'}}, \tag{22}$$

and

Zhang *et al. Chin. J. Mech. Eng.*   (2019) 32:27

Page 9 of 12

Table 3 Peak positions and fitted results for chromium, iron and oxygen from XPS

Potential	Parameter	Fe(0)	Fe$_3$O$_4$	FeO	Fe$_2$O$_3$	FeOOH	Cr(0)	Cr$_2$O$_3$	CrO$_3$	Cr(OH)$_3$	Cr(0)	O^{2-}	OH$^-$
0.2V	E_b/eV	706.7	708.2	709.4	710.9	711.8	574.3	576.8	578.3	577.3	574.3	574.3	576.8
	FWHM	–	–	2.15	4.3	–	–	2.8	–	1.9	–	1.5	1.35
	Atomic concentration	16.01%					10.63%					73.36%	
0.6V	E_b/eV	706.7	708.2	709.4	710.9	711.8	574.3	576.8	578.3	577.3	574.3	574.3	576.8
	FWHM	–	2.82	1.92	3.47	–	–	2.3	2.0	–	–	1.43	1.4
	Atomic concentration	10.75%					11.60%					77.65%	

$$1/Z_{total} = 1/Z_e + 1/Z_h + 1/Z_O + 1/Z_M. \tag{23}$$

Since the rate-controlling step for electrochemical reactions is at interface, and electron transport is fast. Thus the transport of electrons in the passive film is similar to that in metals, it is conceivable that *Ze* equals to *Re*. The impedance for electron holes can also be formulated as a resistor, i.e., $Z_h = R_h$.

The another rate-controlling step is the transport of the anions or anion vacancies across the passive film. Accordingly, the anions at the metal/film (m/f) and film/solution (f/s) interfaces are assumed to be in their equilibrium states. This implies that potential differences at these interfaces affect the concentrations of anions or anion vacancies.

The impedance function for anions and cations can be expressed as

$$Z_O = \sigma_O \omega^{-1/2} - j\sigma_O \omega^{-1/2}, \tag{24}$$

where

$$\sigma_O = RT/F^2\sqrt{32D}\{[C_{V_O}..(m/f)]_{dc}(1-\alpha) - A'\}$$
$$\approx RT/F^2\sqrt{32D}\{[C_{V_O}..(m/f)]_{dc}(1-\alpha)\},$$

and

$$Z_M = \sigma_M \omega^{-1/2} - j\sigma_M \omega^{-1/2}, \tag{25}$$

where $\sigma_M = RT/F^2\sqrt{2x^4D}\{[C_{V_M}x'(m/f)]_{dc}(\alpha - 1)\}$.

At high frequencies where $\omega \gg DK^2$, the total impedance for the passive film Z_f can be reduced to a simple form:

$$Z_f = [1/R + \omega^{1/2}/(1-j)(\sigma_M + \sigma_O)]^{-1}, \tag{26}$$

where $1/R = 1/Z_e + 1/Z_h$.

The diffusivities of oxygen anion and metal cation vacancies in most passive films at room temperature are smaller than 10^{-20} cm^2/s and the *K* value for of passive films is approximately 0.38/cm. Therefore, the relationship of $\omega \gg DK^2$ can be satisfied whenever $\omega > 10^{-13}$

Hz. Accordingly, Eq. (26) is adequate in all practical conditions.

When the electronic current becomes negligible compared with the ionic vacancy currents, Eq. (26) can be further simplified. This situation can be observed when the test solution contains negligible redox species, such as in the absence of an electron exchange reaction at the f/s interface. Accordingly, the total impedance can be expressed

$$Z_f = (\frac{\sigma_O \sigma_M}{\sigma_M + \sigma_O})\omega^{-1/2}(1-j). \tag{27}$$

According to Mott-Schotty analyses and diffusivity of doping concentration, σ_O and σ_M for as-received specimen can be calculated. Fitting and experimental results are shown in Figure 9.

Comparing with the experimental results, there is some error producing after calculating. The error is 37.3%. The main reason is that there are some limitations in PDM I which we use. Firstly, the passive film formed on stainless steel is bi-layer films (proved in Sections 3.4 and 3.5),
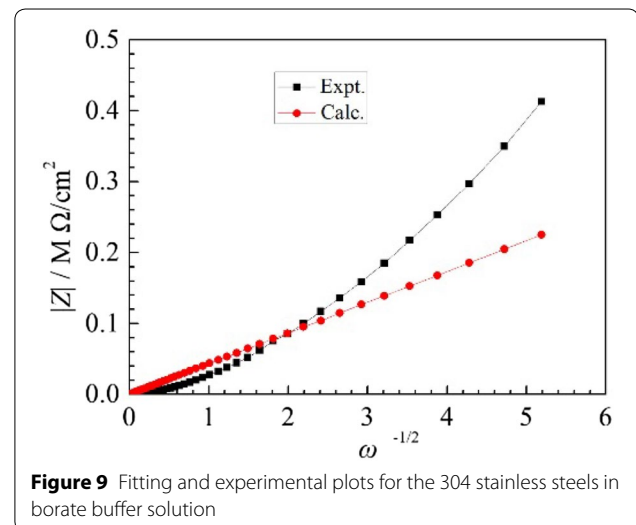

Figure 9 Fitting and experimental plots for the 304 stainless steels in borate buffer solution

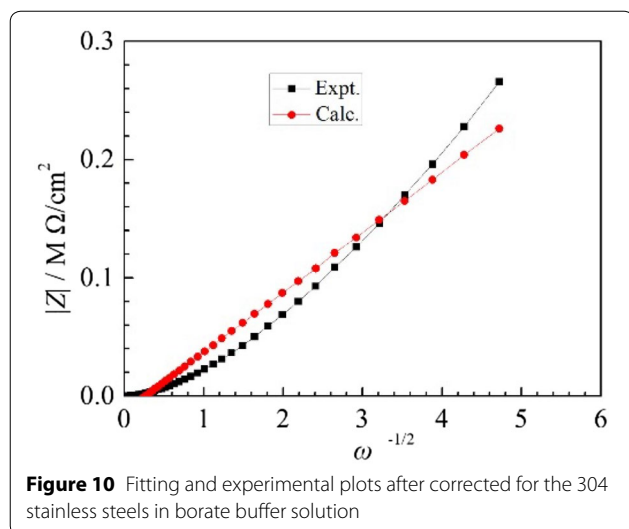Zhang *et al. Chin. J. Mech. Eng.* (2019) 32:27

Page 10 of 12

Figure 10 Fitting and experimental plots after corrected for the 304 stainless steels in borate buffer solution

whereas it was supposed that the passive film is a single layer for calculating. Secondly, there are more defects in the film such as interstitials in addition to cation vacancies and oxygen vacancies. In contrast, the interstitials were neglected in PDM. Thirdly, the outer layer including Fe oxides could dominate the interfacial impedance but not the inner layer [46]. The formula was corrected on the basis of above reasons adding in the metal ion interstitials. So Eq. (26) becomes

$$Z_f = \left[1 \big/ R + \omega^{1/2} \big/ \left(1 - j\right)\left(\sigma_M + \sigma_{M_i} + \sigma_O\right) \right]^{-1}.$$
(28)

The corrected results are shown in Figure 10. And the fitting error decreased to 9.53%.

4 Conclusions

The passivation behavior and corrosion resistance of as-received and sensitized AISI 304 stainless steel were investigated by electrochemical techniques and XPS and DPM. Following results are obtained.

(1) As-received and sensitized AISI 304 stainless steels had both anodic polarization behavior. But pitting corrosion potential of sensitized specimen was a little lower than the as-received one due to precipitated $C_{23}C_6$ along grain boundaries.

(2) The EIS measurements revealed that the impedance diameter of as-received specimens was always higher than that of sensitized specimens at all potentials. The difference in value was bigger in lower potentials than in higher potentials. It was probably that the rate of anodic dissolution was slower than the rate of the oxidation of the Fe^{2+} and Cr^{3+}. The Mott-Schottky results showed sensi-

tized specimen had more defects than as-received one. And N_A was always higher than N_D at specific potential.

(3) The compositions of the passive film were mainly Cr and Fe oxides according to XPS. At 0.2 V_{SCE} the film was enriched in Fe_2O_3 and Cr_2O_3 attributed to the dissolution of Fe and Cr, while CrO_3 and Fe_3O_4 appeared at 0.6 V_{SCE}. And the results of XPS were supported by cyclic voltammograms measurement and Mott-Schottky analysis.

(4) The oxygen vacancy diffusivity is between 10^{-16} and 10^{-17} cm²/s, which is calculated according to PDM and Mott-Schotty analysis.

(5) The impedance response of passive film was certificated by PDM. After correction of the formula, the fitting error decreased from 37.3% to 9.53%.

Authors' Contributions
HL was in charge of the whole trial; YZ wrote the manuscript; QZ, HY, JL assisted with sampling and laboratory analyses. All authors read and approved the final manuscript.

Author Details
[1] Key Laboratory of Aerospace Materials and Performance (Ministry of Education), School of Materials Science and Engineering, Beijing University of Aeronautics and Astronautics, Beijing 100191, China. [2] The Collaborative Innovation Center for Advanced Aero-Engine (CICAAE), Beijing University of Aeronautics and Astronautics, Beijing 100191, China. [3] Beijing Key Laboratory of Advanced Nuclear Materials and Physics, Beijing University of Aeronautics and Astronautics, Beijing 100191, China. [4] China Waterborne Transport Research Institute, Beijing 100088, China. [5] Beijing Key Laboratory of Fine Ceramics, Institute of Nuclear and New Energy Technology, Tsinghua University, Beijing 100084, China.

Authors' Information
Yubo Zhang, born in 1980, is currently a PhD candidate at *School of Materials Science and Engineering, Beihang University, China*, works in *China Waterborne Transport Research Institute*. She received her master degree from *Changchun University of Technology, China*, in 2006. Her research interests include materials surface engineering.

Hongyun Luo, born in 1970, Professor at *School of Materials Science and Engineering, Beihang University, China*. Her research interests include materials surface engineering.

Qunpeng Zhong, born in 1934, Professor at *School of Materials Science and Engineering, Beihang University, China*. He is a failure analysis expert, academician of Chinese Academy of Engineering.

Honghui Yu, born in 1980, is a master candidate at *School of Materials Science and Engineering, Beihang University, China*.

Jinlong Lv, born in 1981, is currently an assistant professor at *School of Engineering, Tohoku University, Japan*. He received his PhD degree from *Beijing University of Aeronautics and Astronautics, China*, in 2014. His research interest focuses on developing advanced supercapacitors electrode and corrosion mechanism of nanocrystalline metal surface.

Zhang *et al. Chin. J. Mech. Eng.* (2019) 32:27

Page 11 of 12

References

[1] M Mamivand, Y Yang, J Busby, et al. Integrated modeling of second phase precipitation in cold-worked 316 stainless steels under irradiation. *Acta Materialia*, 2017, 130: 94–110.

[2] Y Xie, Y Q Wu, Jatuporn Burns, et al. Characterization of stress corrosion cracks in Ni-based weld alloys 52, 52M and 152 grown in high-temperature water. *Materials Characterization*, 2016, 112: 87–97.

[3] D Karthik, S Swaroop. Laser shock peening enhanced corrosion properties in a nickel based Inconel 600 super alloy. *Journal of Alloys and Compounds*, 2017, 694: 1309–1319.

[4] H Y Ha, W G Seo, J Y Park, et al. Influences of Mo on stress corrosion cracking susceptibility of newly developed FeCrMnNiNC-based lean austenitic stainless steels. *Materials Characterization*, 2016, 119: 200–208.

[5] J B Cai, C Yu, R K Shiue, et al. Stress corrosion cracking of austenitic weld deposits in a salt spray environment. *Journal of Nuclear Materials*, 2015, 465: 774–783.

[6] M B Anoop, K Balaji Rao. Safety assessment of austenitic steel nuclear power plant pipelines against stress corrosion cracking in the presence of hybrid uncertainties. *International Journal of Pressure Vessels & Piping*, 2008, 85: 238–247.

[7] R Leiva-García, M J Muñoz-Portero, J García-Antón. Corrosion behavior of sensitized and unsensitized Alloy 900 (UNS 1.4462) in concentrated aqueous lithium bromide solutions at different temperatures. *Corrosion Science*, 2010, 52: 950–959.

[8] Q Guo, J H Liu, M Yu, et al. Effect of passive film on mechanical properties of martensitic stainless steel 15-5PH in a neutral NaCl solution. *Applied Surface Science*, 2015, 327: 313–320.

[9] S Sharifi-Asl, F X Mao, P Lu, et al. Exploration of the effect of chloride ion concentration and temperature on pitting corrosion of carbon steel in saturated Ca(OH)$_2$ solution. *Corrosion Science*, 2015, 98: 708–715.

[10] R Nishimura. Characterization and perspective of stress corrosion cracking of austenitic stainless steels (type 304 and type 316) in acid solutions using constant load method. *Corrosion Science*, 2007, 49: 81–91.

[11] H Sun, X Q Wu, E H Han. Effects of temperature on the oxide film properties of 304 stainless steel in high temperature lithium borate buffer solution. *Corrosion Science*, 2009, 51: 2840–2847.

[12] J B Huang, X Q Wu, E H Han, Influence of pH on electrochemical properties of passive films formed on Alloy 690 in high temperature aqueous environments. *Corrosion Science*, 2009, 51: 2976–2982.

[13] Y Li, Y F Cheng. Passive film growth on carbon steel and its nanoscale features at various passivating potentials. *Applied Surface Science,* 2017, 396: 144–153.

[14] H Luo, H Z Su, C F Dong, et al. Passivation and electrochemical behavior of 316L stainless steel in chlorinated simulated concrete pore solution. *Applied Surface Science*, 2017, 400: 38–48.

[15] A Fattah-alhosseini, M A Golozar, A Saatchi, et al. Effect of solution concentration on semiconducting properties of passive films formed on austenitic stainless steels. *Corrosion Science*, 2010, 52: 205–209.

[16] Y C Zhang, D D Macdonald. Passivity breakdown on AISI Type 403 stainless steel in chloride-containing borate buffer solution. *Corrosion Science*, 2006, 48: 381–3823.

[17] I Nicic, D D Macdonald. The passivity of Type 316L stainless steel in borate buffer solution. *Journal of Nuclear Materials*, 2008, 379: 54–58.

[18] J Congleton. The effect of applied potential on the stress corrosion cracking of sensitized Type 316 stainless steel in high temperature water. *Corrosion Science*, 1995, 37: 429–444.

[19] M Kumagai, S T Myung, Y Katada, et al. Stability of type 310S stainless steel bipolar plates tested at various current densities in proton exchange membrane fuel cells. *Electrochimica Acta*, 2016, 211: 754–760.

[20] I Diaz, J F Martinez-Lerma, R Montoya, et al. Study of overall and local electrochemical responses of oxide films grown on CoCr alloy under biological environments. *Bioelectrochemistry*, 2017, 115: 1–10.

[21] A Kocijan, Č Donik, M Jenko. Electrochemical and XPS studies of the passive film formed on stainless steels in borate buffer and chloride solutions. *Corrosion Science*, 2007, 49: 2083–2098.

[22] W Fredriksson, S Malmgren, T Gustafsson, et al. Full depth profile of passive films on 316L stainless steel based on high resolution HAXPES in combination with ARXPS. *Applied Surface Science*, 2012, 258: 5790–5797.

[23] V Vignal, O Delrue, O Heintz, et al. Influence of the passive film properties and residual stresses on the micro-electrochemical behavior of duplex stainless steels. *Electrochimica Acta*, 2010, 55: 7118–7125.

[24] A Abou-Elazm, R Abdel-Karim, I Elmahallawi, et al. Correlation between the degree of sensitization and stress corrosion cracking susceptibility of type 304H stainless steel. *Corrosion Science*, 2009, 51: 203–208.

[25] C A Huang, Y Z Chang, S C Chen. The electrochemical behavior of austenitic stainless steel with different degrees of sensitization in the transpassive potential region in 1 M H2SO4 containing chloride. *Corrosion Science*, 2004, 46: 1501–1513.

[26] L Hamadou, A Kadri, N Benbrahim. Impedance investigation of thermally formed oxide films on AISI 304L stainless steel. *Corrosion Science*, 2009, 52: 859–864.

[27] Y Gui, Z J Zheng, Y Gao. The bi-layer structure and the higher compactness of a passive film on nanocrystalline 304 stainless steel. *Thin Solid Films*, 2016, 599: 64–71.

[28] Z C Feng, X Q Cheng. Passivity of 316L stainless steel in borate buffer solution studied by Mott–Schottky analysis, atomic absorption spectrometry and X-ray photoelectron spectroscopy. *Corrosion Science*, 2010, 52: 3646–3653.

[29] T L S L Wijesinghe, D J Blackwood. Characterisation of passive films on 300 series stainless steels. *Applied Surface Science*, 2006, 253: 1006–1009.

[30] P Córdoba-Torres. Relationship between constant-phase element (CPE) parameters and physical properties of films with a distributed resistivity. *Electrochimica Acta*, 2017, 225: 592–604.

[31] Y X Qiao, Y G Zheng. Electrochemical behaviour of high nitrogen stainless steel in acidic solutions. *Corrosion Science*, 2009, 51: 979–986.

[32] N E Hakiki. Comparative study of structural and semiconducting properties of passive films and thermally grown oxides on AISI 304 stainless steel. *Corrosion Science*, 2011, 53: 2688–2699.

[33] Arash Fattah-alhosseini, Ali Reza Ansari, Yousef Mazaheri, et al. Effect of immersion time on the passive and electrochemical response of annealed and nano-grained commercial pure titanium in Ringer's physiological solution at 37 ℃. *Materials Science & Engineering C*, 2017, 71: 771–779.

[34] S H Zhang, R X Shi, Y Tan. Corrosion behavior of the oxide films modified with zincizing treatment on AISI 1020 steel. *Journal of Alloys & Compounds*, 2017, 711: 155–161.

[35] S Marcelin, B Ter-Ovanessian, B Normand. Electronic properties of passive films from the multi-frequency Mott–Schottky and power-law coupled approach. *Electrochemistry Communications*, 2016, 66: 62–65.

[36] J Williamson, O B Isgor. The effect of simulated concrete pore solution composition and chlorides on the electronic properties of passive films on carbon steel rebar. *Corrosion Science*, 2016, 106: 82–95.

[37] S Ningshen, U Kamachi Mudali. Semiconducting and passive film properties of nitrogen- containing type 316LN stainless steels. *Corrosion Science*, 2007, 49: 481–496.

[38] D D Macdonald. Theoretical investigation of the evolution of the passive state on Alloy 22 in acidified, saturated brine under open circuit conditions. *Electrochimica Acta*, 2011, 56: 7411–7420.

[39] T L Sudesh, L Wijesinghe, D J Blackwood. Characterisation of passive films on 300 series stainless steels. *Applied Surface Science*, 2006, 253: 1006–1009.

[40] Y K Bai, Y H Ling, W S Lai, et al. Electrochemical properties of the passive film on bulk Zr–Fe–Cr intermetallic fabricated by spark plasma sintering. *Applied Surface Science*, 2016, 388: 212–222.

[41] S Virtanen, M Buchler. Electrochemical behaviour of surface films formed on Fe in chromate solutions. *Corrosion Science*, 2003, 45: 1405–1419.

[42] D C Kong, A N Xu, C F Dong, et al. Electrochemical investigation and ab initio computation of passive film properties on copper in anaerobic sulphide solutions. *Corrosion Science*, 2017, 116: 34–43.

[43] E Sikora, J Sikora, D D Macdonald. A new method for estimating the diffusivities of vacancies in passive films. *Electrochimica Acta*, 1996, 41: 783–789.

[44] Y F Cheng, C Yang, J L Luo. Determination of the diffusivity of point defects in passive films on carbon steel. *Thin Solid Films*, 2002, 416: 169–173.

Zhang *et al. Chin. J. Mech. Eng.*   *(2019) 32:27*

Page 12 of 12

[45] I F Lin, C Y Chao, D D Macdonald. A point defect model for anodic passive films III. impedance pesponse. *Journal of the Electrochemical Society*, 1982, 29: 1874–1879.

[46] D D Macdonald. The history of the point defect model for the passive state: A brief review of film growth aspects. *Electrochimica Acta*, 2011, 56: 1761–1772.